

Collective excitations in jammed states: ultrafast defect propagation and finite-size scaling

Alexander P. Antonov,¹ David Voráč,² Artem Ryabov,² and Philipp Maass¹

¹*Universität Osnabrück, Fachbereich Physik,
Barbarastraße 7, D-49076 Osnabrück, Germany*

²*Charles University, Faculty of Mathematics and Physics,
Department of Macromolecular Physics,
V Holešovičkách 2, CZ-18000 Praha 8, Czech Republic*

(Dated: November 15, 2022)

Abstract

In crowded systems, particle currents can be mediated by propagating collective excitations which are generated as rare events, are localized and have a finite lifetime. The theoretical description of such excitations is hampered by the problem of identifying complex many-particle transition states, calculation of their free energies, and the evaluation of propagation mechanisms and velocities. Here we show that these problems can be tackled for a highly jammed system of hard spheres in a periodic potential. We derive generation rates of collective excitations, their anomalously high velocities, explain the occurrence of an apparent jamming transition and its strong dependence on the system size. The particle currents follow a scaling behavior, where for small systems the current is proportional to the generation rate and for large systems given by the geometric mean of the generation rate and velocity. Our theoretical approach is widely applicable to dense nonequilibrium systems in confined geometries. It provides new perspectives for studying dynamics of collective excitations in experiments.

I. INTRODUCTION

In molecular transport at the nanoscale, spatial confinements slow down particle motion that ultimately can become arrested in a jammed state. The slowing down is in particular observed at high particle densities in single-file dynamics, where particles cannot overtake each other [1, 2]. Such transport ubiquitously occurs in biological traffic [3, 4], like in the protein synthesis by ribosomes [5] and molecular motor motion along filaments [6, 7]. It is highly relevant also for nanotechnology and chemical engineering including catalytic processes in zeolites [8], molecular sieves, as well as for control and steering of flows in nanotubes [9, 10], and membrane channels and pores [11–13].

Paradigmatic models for biological single-file transport are the asymmetric simple exclusion process (ASEP) and its variants [14–20]. In ASEP [14, 15], a particle current is induced by letting particles hop between neighboring sites of a one-dimensional lattice with a bias in one direction. Each lattice site can be occupied by at most one particle, reflecting hardcore (steric) interactions. Over the last decades, this simple process has become a fundamental model for nonequilibrium statistical mechanics. It provides one of the rare cases, where the statistical mechanics of nonequilibrium steady states can be derived exactly. Thanks to these exact results, many intriguing phenomena could be understood on a firm basis. Most prominent is perhaps the occurrence of phase transitions, which cannot appear in equilibrium one-dimensional systems. These phase transitions are related to the nonlinear dependence of the current on the particle density [21–23]. In ASEP, the nonlinear current-density relation is a direct consequence of particle hops becoming increasingly blocked with higher density. This eventually leads to jamming when the number of particles equals the number of lattice sites (filling factor one).

For single-file transport in zeolites, membrane channels and pores, the coarse-grained lattice description is less appropriate. Recently, we have shown that the dynamics in these systems should be very different from ASEP-like behavior [24–26]. Inspired by ASEP, we suggested the Brownian asymmetric exclusion process (BASEP) [24] to model driven single-file motion in periodic potentials. In BASEP, hard-sphere interacting particles with diameter σ are driven by a constant external force f in a cosine potential with wavelength λ . In connection with a coarse-grained lattice description, one may think of the potential wells to represent the lattice sites and the force f to give rise to preferential hopping of particles

between neighboring wells. However, while the wavelength λ of the periodic potential plays the role of a lattice constant, the particle size σ turns out to be a very important length scale that leads to novel collective effects that are absent in a corresponding lattice description.

The BASEP is useful to interpret nonequilibrium phenomena studied experimentally in soft matter and microfluidic systems, where the particle size has a strong influence on the dynamics. It shows various interesting features, as many-particle induced current enhancement with respect to noninteracting particles, current suppression due to mutual particle blocking, and commensurability effects when σ becomes close to multiples of the wavelength λ of the periodic potential. In recent experiments, the BASEP was helpful to understand fundamental differences between flow- and force-driven single-file transport of colloids in fluidic environments [27].

Here, we show that an apparent jamming transition occurs in BASEP for $\rho = 1$, when σ approaches values of about 0.75λ . This transition is demonstrated in Fig. 1 for a periodic system with 20 potential wells. It manifests itself in a current decreasing by several orders of magnitude when σ is increased from 0.6 to 0.75λ . An experimental realization of this setting [27] is sketched in the inset of Fig. 1. In the experiments, the current would drop essentially to zero, like in a jamming transition with complete arrest of particle flow.

Considering the complete filling of all the potential wells, it may appear surprising that particle flow can still be present at large particle diameters σ . However, transport in the apparently jammed phase is still possible by cluster-like defects with a certain lifetime that propagate in the direction of the drag force. We refer to them as collective excitations [28], which on entropic reasons must occur in any crowded system, albeit rarely.

These localized excitations are different from low-frequency wave-like collective excitations, which also occur in hard-sphere systems [29]. They are defects composed of several particles and are generated via well-defined transition states by overcoming free energy barriers that depend on the particle size σ . After formation, the defects propagate with surprisingly high velocity. The defect lifetimes depend strongly on the system size L , which gives rise to pronounced variation of the defect-mediated currents with L . In particular, the apparent jamming transition becomes less pronounced with increasing L . The sensitive dependence of the currents on both L and σ follows a scaling law.

Generally, it is very difficult to gain a thorough understanding of the generation and motion of collective excitations in crowded systems, because of the complex particle configurations

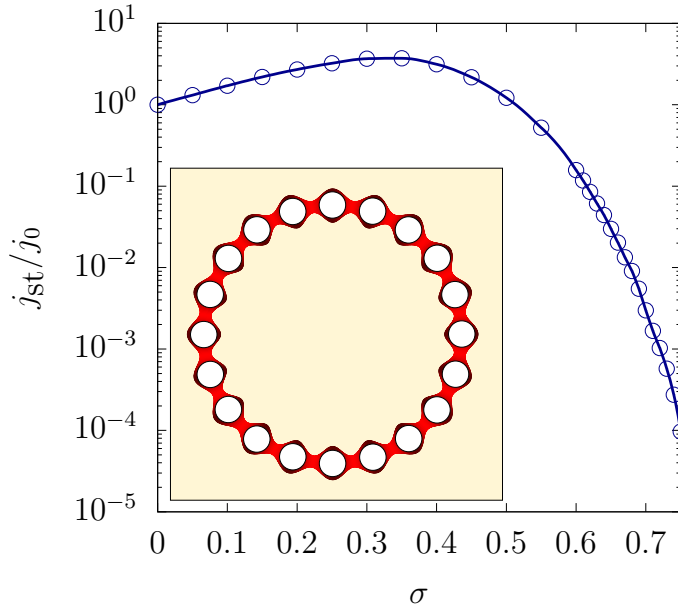


FIG. 1. Normalized steady-state current j_{st}/j_0 for $N = 20$ hard spheres as a function of their diameter σ . The spheres are performing an overdamped Brownian motion in the cosine potential $U(x) = (U_0/2) \cos(2\pi x/\lambda)$ with N potential wells (filling factor one) subject to periodic boundary conditions. They are dragged by a constant force f . The normalization j_0 refers to the current of noninteracting particles. Symbols mark results from Brownian dynamics simulations and the line is drawn as a guide for the eye. Parameters are $U_0 = 6$ and $f = 0.2$ in the chosen units ($k_B T = 1$, $\lambda = 1$). The inset illustrates an experimental realization of the model [27]: 20 microparticles are confined to 20 optical traps (potential wells). Particle transport along the ring becomes possible after creating an empty potential well (hole) by a thermal excitation.

involved in these processes. Also, it is hard to study collective excitations in experiments. The system in Fig. 1 is suitable to meet both these theoretical and experimental challenges.

II. DEFECT-MEDIATED TRANSPORT

The Brownian dynamics of N particles in BASEP is given by the Langevin equations

$$\frac{dx_i}{dt} = \mu (f - U'(x_i)) + \sqrt{2D} \eta_i(t), \quad i = 1, \dots, N, \quad (1)$$

where μ is the particle mobility, $D = k_B T \mu$ is the bare diffusion coefficient of a single particle in a flat potential with $k_B T$ the thermal energy, and $\eta_i(t)$ are Gaussian white noise processes

with zero mean and correlations $\langle \eta_i(t)\eta_j(t') \rangle = \delta_{ij}\delta(t-t')$. The function

$$U(x) = \frac{U_0}{2} \cos\left(\frac{2\pi x}{\lambda}\right) \quad (2)$$

is the external λ -periodic potential, where $U_0 \gg k_B T$, and the constant force f is driving the particles. Due to the hard-sphere interaction, the distance between neighboring particles cannot be smaller than σ and the particles keep their order (single-file transport). The filling factor of the potential wells is $\rho = N\lambda/L$, where L is the system length.

Several fast simulation algorithms have been developed in the past to tackle the hard-sphere interactions in Brownian dynamics simulations [30–34]. When we refer to simulation results in the following, we always used the algorithm given by Scala et al. [31]. This is an event-driven scheme [35] and details of our implementation can be found in Ref. [36]. A new approach to this problem, which addresses the theoretical basis of a treatment in arbitrary external force fields, will be given in Ref. [37].

We applied periodic boundary conditions for a system size L being an integer multiple of λ . As units of energy, length and time, we used $k_B T$, λ and λ^2/D , respectively. The potential amplitude is fixed to $U_0 = 6$ and this value much larger than the thermal energy implies that a single-particle motion in the periodic potential would be a thermally activated hopping on the scale of the Kramers’ time. The drag force is fixed to 0.2, i.e., $f\lambda/k_B T = 0.2$, meaning that we consider a weak driving much below the critical “tilting force” $f_c = \pi U_0/\lambda \cong 18.8$, above which potential minima would no longer be present.

The apparent jamming transition in Fig. 1 occurs for filling factor $\rho = 1$ and is reflected in a rapid decrease of the steady-state current j_{st} with growing particle size when σ becomes larger than 0.6. For small particle diameters, j_{st} increases because of a barrier reduction effect discussed earlier [24, 26, 38]. Here we focus our study on the regime $\sigma > 0.6$ and the defect-mediated transport associated with the apparent jamming transition. In the following, we characterize the defects and calculate defect generation rates and lifetimes, which in turn enable us to predict transport properties.

A. Defect generation rate

In a system with filling factor $\rho = 1$, the energetically preferred particle configuration would be the crystalline type shown in Fig. 2(a): all particles are residing close to the minima

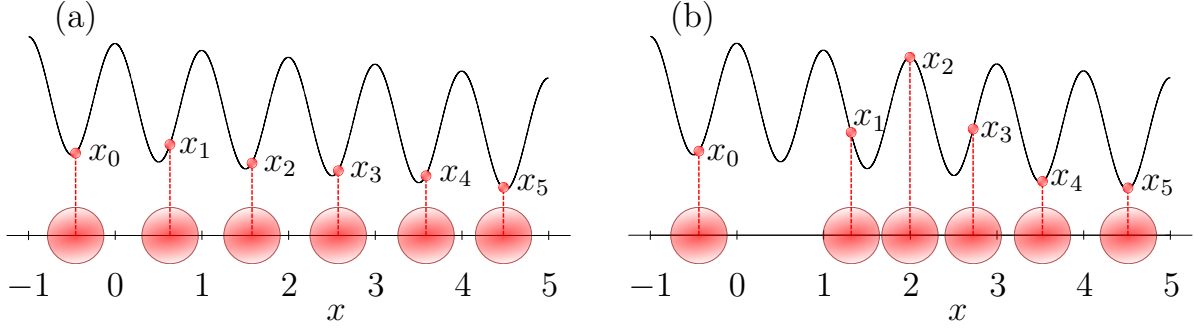


FIG. 2. Sketch of local configurations of six hard spheres with diameter $\sigma = 0.65$ in the tilted potential $U(x) - fx$. In (a) a typical state is shown, where the particles are located close to positions of mechanical equilibria. These positions are at $m + 1/2 + \xi$, $m = -1, 0, \dots$, where ξ is given in Eq. (3) and has the small value $\xi \cong 0.017$ for our parameters $U_0 = 6$ and $f = 0.2$. In (b) a rare transition state is depicted, where a hole is present around the minimum at $1/2 + \xi$ (empty well between maxima at $-\xi$ and $1 - \xi$). The transition state is formed by two particles (2-particle transition state): the first particle to the right of the hole has not returned to the empty potential well, while the second particle is located at the maximum at $2 - \xi$.

of the tilted periodic potential $U(x) - fx$. The minima and maxima of the tilted potential are at positions $m - \xi$ and $m + 1/2 + \xi$ with m an integer, respectively, where

$$\xi = \frac{1}{2\pi} \arcsin\left(\frac{\pi f}{U_0}\right). \quad (3)$$

If the particles have a diameter $\sigma > 0.5$, double occupancies of potential wells are highly improbable. At first sight, the system appears to be frozen and it is difficult to imagine how a weak driving force can generate a current. However, thermal excitations can lead to defects, where a particle escapes a potential well and leaves an unoccupied well behind, as illustrated for particle 1 in Fig. 2(b). We call an unoccupied potential well a hole.

After hole formation, several particles form a defect next to the hole. This defect can disappear after a short transient time, if the particle that has escaped the potential well and left the hole behind, returns to the well, see the particle trajectory marked in green in Fig. 3(a). More interesting is the case where the defect starts to propagate in the bias direction, see Fig. 3(b). On average over time, the hole then moves slowly against the drag force due to a biased hopping-like motion of the particles next to it.

The reason for the different time evolutions after hole formation is that in Fig. 2(b) a

transition state for a propagating defect is generated, while this is not the case in Fig. 2(a). In the transition state, the second particle to the right of the hole [red trajectory in Fig. 2(b)] reaches the second potential maximum from the hole in bias direction (position 3 in the figure), while the hole is still present. The time instant, when this happens, is indicated by the vertical line. We found that such event is a prerequisite for obtaining a propagating defect shown in Fig. 4(a).

We consider a propagating defect generated by two “excited particles” as a one with a 2-particle transition state. For larger particle diameters, also n -particle transition states with $n = 3, 4, \dots$ can occur. In these transition states, particle n must reach the potential maximum at a distance of $1/2 + (n - 1)$ wavelengths from the hole, and particles $1, \dots, (n - 1)$ all need to have passed one potential barrier. If the hole is located at $x = 1/2 + \xi$ as in Fig. 2(b), the coordinates x_1, \dots, x_{n-1} of these particles must satisfy the conditions

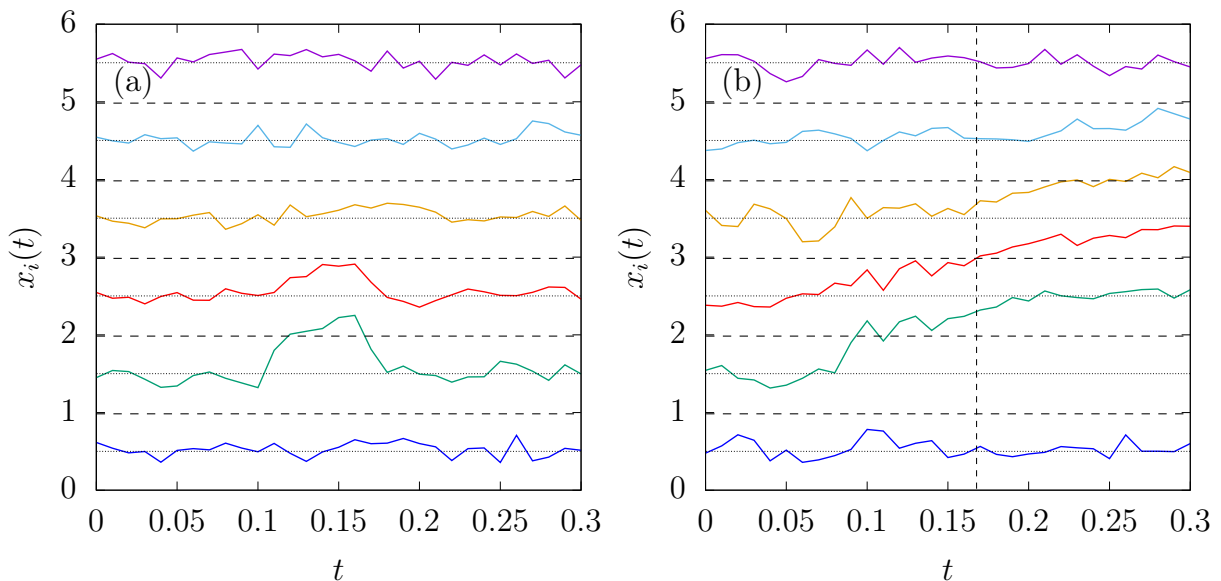


FIG. 3. Simulated particle trajectories for $\sigma = 0.65$ that illustrate possible system evolutions right after a hole formation. Horizontal dotted and dashed lines mark minima and maxima of the tilted potential, respectively. In (a) a hole appears at time $t \simeq 0.12$ and is refilled at $t \simeq 0.17$ (see trajectory marked in green). In (b) a 2-particle transition state for a propagating defect forms at a time indicated by the vertical dashed line. This transition state corresponds to the one depicted schematically in Fig. 2(b). The propagation of the defect formed after its generation is displayed in Fig. 4(a).

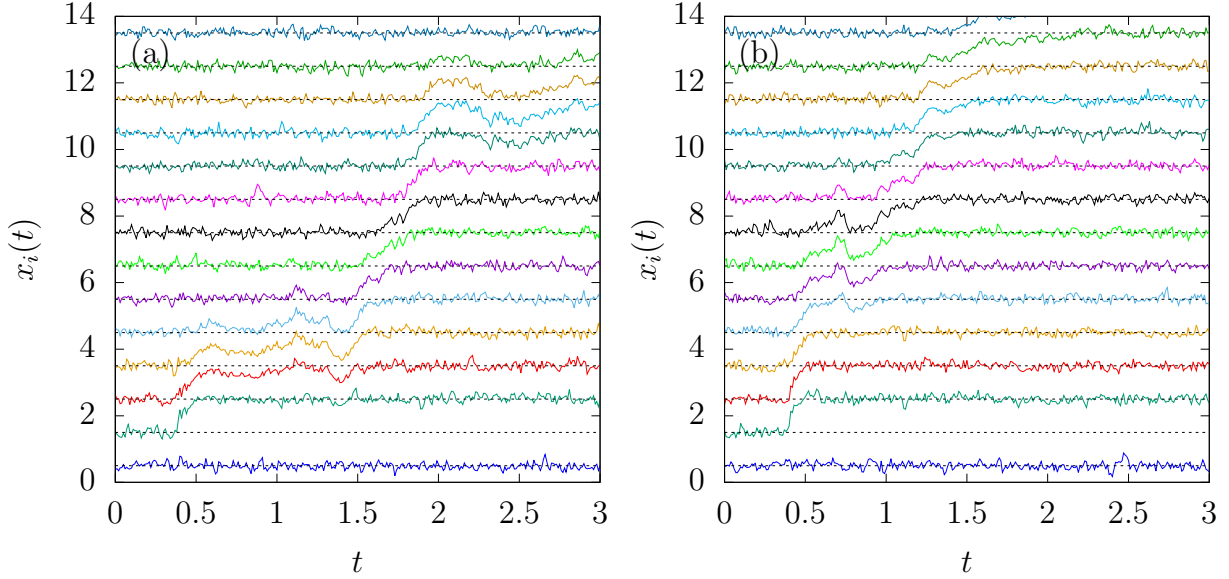


FIG. 4. Propagating defects for (a) $\sigma = 0.65$ and (b) $\sigma = 0.75$. In (a) the defect is generated via the 2-particle transition state displayed in Fig. 3(b), while for the larger particle diameter in (b) the generation of the defect is via a 3-particle transition state at time $t \simeq 0.5$. The propagating defect in (b) involves a larger number of particles and moves faster than the one in (a).

$x_i > (i - \xi)$, $i = 1, \dots, (n - 1)$. This defines the n -particle transition state for generating a propagating defect.

For calculating the free energy $F_n^\ddagger(\sigma)$ of the transition state and the free energy $F_n^0(\sigma)$ of a corresponding reference state, we consider two boundary particles placed at fixed positions of mechanical equilibrium. To be specific, the boundary particle to the left is at position $x_b^- = -1/2 + \xi$ and the boundary particle to the right at position $x_b^+ = x_b^- + 2n + 1$. This implies that we place these boundary particles at a distance of $(2n + 1)$ wavelengths, which allows $2n$ particles to occupy $2n$ different potential wells in the reference state. We found that it is sufficient to consider n additional particles to the right of the particle n at the potential maximum, because taking a larger number is not affecting the results for $F_n^\ddagger(\sigma)$ and $F_n^0(\sigma)$.

In the transition state, the particle n must be at the position $x_n^\ddagger = n - \xi$. Therefore, the position of the particle n is also fixed in the reference state, but now at the position of mechanical equilibrium at $x_n^0 = n - 1/2 + \xi$. The free energy of the reference state then is

$F_n^0(\sigma) = -\ln Z_n^0(\sigma)$ with the partition sum

$$Z_n^0(\sigma) = \exp\left\{-[U(x_n^0) - fx_n^0]\right\} \int_{x_n^0+\sigma}^{x_b^+-n\sigma} dx_{n+1} \int_{x_{n+1}+\sigma}^{x_b^+-(n-1)\sigma} dx_{n+2} \dots \int_{x_{2n-1}+\sigma}^{x_b^+-\sigma} dx_{2n} \quad (4)$$

$$\times \int_{x_b^++(n-1)\sigma}^{x_n^0-\sigma} dx_{n-1} \int_{x_b^++(n-2)\sigma}^{x_{n-1}-\sigma} dx_{n-2} \dots \int_{x_b^-+2\sigma}^{x_3-\sigma} dx_2 \int_{x_b^-+\sigma}^{x_2-\sigma} dx_1 \exp\left\{-\sum_{j=1, j \neq n}^{2n} [U(x_j) - fx_j]\right\}.$$

In the transition state, in addition to setting $x_n^\ddagger = n - \xi$, we must require the potential well covering the interval $[-\xi, 1 - \xi]$ to be empty (representing a hole). The first $(n - 1)$ particles occupy positions in the interval $[j - \xi, x_{j+1} - \sigma]$, $j = 1, \dots, (n-1)$, and the remaining n particles occupy positions in the interval $[x_{j-1} + \sigma, x_b^+ - (2n + 1 - j)\sigma]$, $j = (n+1), \dots, 2n$. Accordingly, the free energy of the transition state is $F_n^\ddagger(\sigma) = -\ln Z_n^\ddagger(\sigma)$ with

$$Z_n^\ddagger(\sigma) = \exp\left\{-[U(x_n^\ddagger) - fx_n^\ddagger]\right\} \int_{x_n^\ddagger+\sigma}^{x_b^+-n\sigma} dx_{n+1} \int_{x_{n+1}+\sigma}^{x_b^+-(n-1)\sigma} dx_{n+2} \dots \int_{x_{2n-1}+\sigma}^{x_b^+-\sigma} dx_{2n} \quad (5)$$

$$\times \int_{n-1-\xi}^{x_n^\ddagger-\sigma} dx_{n-1} \int_{n-2-\xi}^{x_{n-1}-\sigma} dx_{n-2} \dots \int_{2-\xi}^{x_3-\sigma} dx_2 \int_{1-\xi}^{x_2-\sigma} dx_1 \exp\left\{-\sum_{j=1, j \neq n}^{2n} [U(x_j) - fx_j]\right\}.$$

The free energy barrier between the transition and reference state yields the rate $\lambda_n(\sigma)$ for generating a propagating defect via an n -particle transition state,

$$\lambda_n(\sigma) = \nu \exp[-(F_n^\ddagger(\sigma) - F_n^0(\sigma))] = \nu \frac{Z_n^\ddagger(\sigma)}{Z_n^0(\sigma)}. \quad (6)$$

Here, ν is a bare rate, which should be of the order of D/λ^2 , i.e., one in our units.

Figure 5 (left axis) shows λ_2 , λ_3 and λ_4 as functions of σ in comparison with simulated data, where we performed the integrations in Eqs. (4) and (5) numerically and set $\nu = 1$. In the simulations, we determined λ_{gen} by counting the mean number \bar{N}_{def} of propagating defects in a large time interval Δt in the non-equilibrium steady state, yielding $\lambda_{\text{gen}} = \bar{N}_{\text{def}}/\Delta t$. The data are plotted for the range $\sigma \in [0.6, 0.75]$, where we could determine the generation rate λ_{gen} of propagating defects with reliable accuracy. Note that the formation of a defect is a rare thermally activated event and that λ_{gen} decreases faster than exponentially with σ . In the considered σ -interval, λ_{gen} falls by about three orders of magnitude, reaching extremely small values for $\sigma \gtrsim 0.7$.

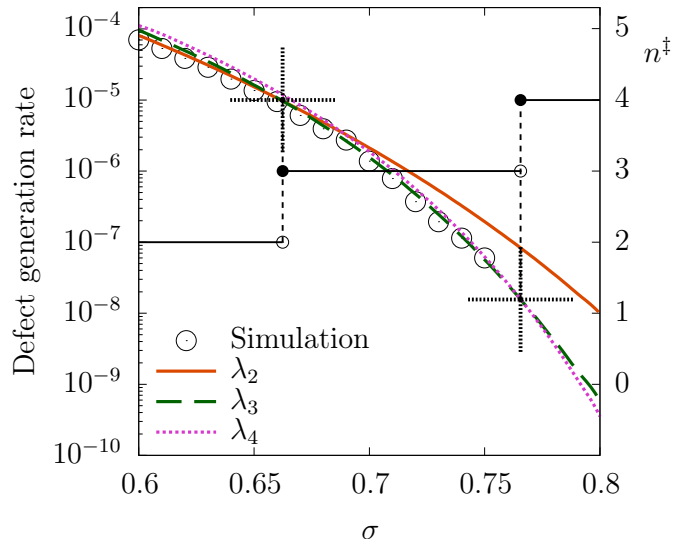


FIG. 5. Defect generation rates (left axis) for different particle diameters σ . The rates λ_n were calculated from Eq. (6). The number n^\ddagger of particles involved in the transition state (right axis) increases with σ in a staircase-like manner. The steps of this staircase are determined by Eq. (8) and occur at particle diameters, where lines for different λ_n intersect, as indicated by the crosses.

The simulated data of λ_{gen} in Fig. 5 agree well with the calculated λ_2 for $\sigma \lesssim 0.66$ and with the calculated λ_3 for $\sigma \gtrsim 0.66$. In fact, we found that the smaller of the two calculated rates gives a very good prediction of λ_{gen} , i.e.,

$$\lambda_{\text{gen}}(\sigma) \cong \min_n \{\lambda_n(\sigma)\}. \quad (7)$$

This can be formulated as a maximum free energy barrier principle: for given σ , the particle number n^\ddagger defining the transition state follows by maximizing the free energy barrier $\Delta F_n^\ddagger(\sigma) = [F_n^\ddagger(\sigma) - F_n^0(\sigma)]$ with respect to n ,

$$n^\ddagger(\sigma) = \operatorname{argmax}_n \{\Delta F_n^\ddagger(\sigma)\}. \quad (8)$$

Its generation rate then is $\lambda_{\text{gen}} = \lambda_{n^\ddagger}$. The staircase-like increase of n^\ddagger with the particle diameter predicted by the maximum free energy barrier principle is displayed in Fig. 5 (right axis). The change from the 2-particle to the 3-particle transition state should occur at $\sigma \cong 0.66$. The examples of defects generation and propagation shown in Fig. 4 are in agreement with this prediction.

One may ask why a principle of maximum instead of minimum free energy barrier is present. This has the following explanation. First, we note that to create an n -particle

transition state, the $(n - k)$ -particle transition states with $k = 1, \dots, (n - 2)$ need to be created as intermediate states. Second, we point out that for creating a propagating defect, the hole must not refill, i.e., a stabilized hole needs to be created. For smaller σ , it is enough to have one single-occupied well to the right of the hole for stabilizing it. This explains why for $0.6 < \sigma \lesssim 0.66$ in Fig. 5 the rate λ_2 is giving λ_{gen} : the 2-particle transition state must be created first and it is sufficient to obtain a stabilized hole and a propagating defect. When increasing σ , the particles in the double-occupied next-neighboring well to the right have a higher tendency to push the particle from the neighboring well back to the hole. The hole therefore becomes stabilized only after two single-occupied wells are created right of it. This leads to the three-particle transition state as the relevant one for generating a propagating defect and explains why the rate λ_3 is giving λ_{gen} for $0.66 \lesssim \sigma < 0.75$: the 2-particle transition state must be created first, but it is not sufficient for obtaining a stabilized hole, as the two particles in the double-occupied next-neighboring well of the hole are pushing the particle back into the next-neighboring well. When increasing σ further, we conjecture that this mechanism will proceed: the number of single-occupied wells needed to stabilize the hole increases. This protects the hole against refilling from the right. We could not confirm this mechanism for $\sigma > 0.75$ in the simulations as the events of propagating defect generation become too rare.

The very strong decrease of λ_{gen} with σ in Fig. 5 suggests that it is responsible for the apparent jamming transition seen in Fig. 1. However, the defect-mediated current is not only dependent on the generation rate of the defects but also on the defect velocity. To obtain a complete picture we thus need to understand the defect velocities and their dependence on σ .

B. Defect velocity

To calculate the defect velocity v_d in simulations, we recorded the time instant t_{gen} when a propagating defect is generated and the time instant t_{ann} when this defect becomes annihilated due to recombination with a hole. In the time interval $[t_{\text{gen}}, t_{\text{ann}}]$, we followed the trajectory of the double-occupied well in the defect. Then we excluded the initial period $[t_{\text{gen}}, t_{\text{gen}} + 1]$ because right after the defect generation, the propagation of the double-occupied well is much faster than on average, see also the defect initiation periods in Figs. 4(a) and (b). A similar effect occurs before the recombination with a hole and we therefore excluded also

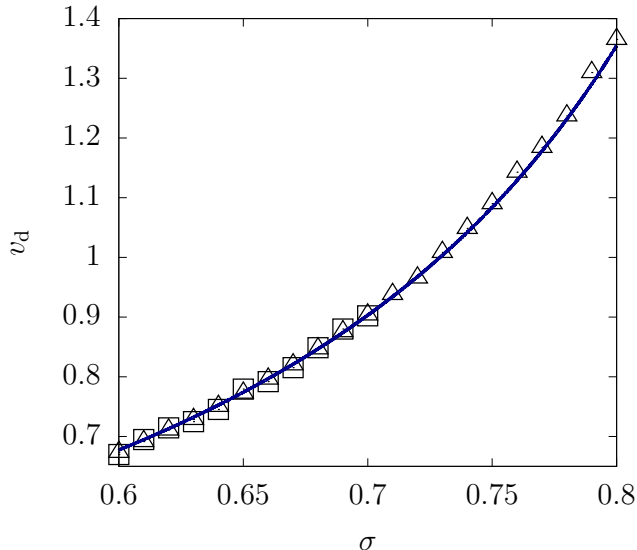


FIG. 6. Velocity of propagating defects in dependence of the particle diameter. The squares show simulation results for a system with filling factor one, and the triangles represent the results from the inserted particle method (11 particles in a system with 10 potential wells). The line refers to the theoretical prediction given by Eq. (9) with $\alpha = 1.35$.

the time interval $[t_{\text{ann}} - 1, t_{\text{ann}}]$ from the analysis. The defect velocity is obtained from the distance traveled by the double-occupied well within the considered time interval.

In this method, an averaging of v_d over many individual defect trajectories requires a high computational effort because of the low defect generation rate, in particular at larger σ . A more convenient method is to create a defect artificially by inserting an additional particle into the system with filling factor one. This immediately creates one defect and allows to calculate v_d from mean travelled distances per time. Results from both methods agree, see Fig. 6. In principle, it would be possible to create defects also by inserting more than one particle into the system with filling factor one. In that case, however, more than one defect can form. This does not only complicate the determination of the velocities of each defect but the defect velocities can then be influenced also by effective defect-defect interactions.

The dependence of v_d on σ in Fig. 6 is very weak compared to the change of λ_{gen} in Fig. 5, note the different scales of the vertical axes. While λ_{gen} decreases by more than three orders of magnitude when σ is increased from 0.6 to 0.75, the defect velocity increases by a factor of about 1.5 only. What is remarkable is the magnitude of v_d , which is about hundred times larger than the velocity $v_0 \cong 8.4 \times 10^{-3}$ of noninteracting particles (this can be calculated

based on an exact result for a single particle, see [39, 40]). It is even about four times larger than the velocity $f = 0.2$ ($\mu = 1$ for the chosen units) of independent particles in a flat potential.

To understand the behavior of v_d , let us note that during the defect motion compact cluster-like structures appear where four or more particles are nearly in contact with each other, see Figs. 4(a) and (b). This motivates the following rough estimation: let us consider a cluster of $(n + 1)$ particles in contact with each other, where the first (leftmost) particle is at the minimum of the tilted potential and the remaining n particles are moving as a compact cluster until the second particle reaches a point of mechanical equilibrium. To reach this point, the cluster has to move a distance $(1 - \sigma)$. After reaching it, the whole defect is shifted by one wavelength, because the second particle is now adopting the role of the first particle. Hence we can say that the defect velocity is $v_d(\sigma) = 1/t_\sigma$, where t_σ is the mean time of the cluster to move a distance $(1 - \sigma)$.

The cluster center follows a Brownian motion in a tilted cosine potential with the same wavelength and drag force, but with a reduced amplitude $(U_0/n) \sin(n\pi\sigma)/\sin(\pi\sigma)$ of the external potential [41]. Due to the factor $1/n$, this amplitude is of the order of $k_B T = 1$ for cluster sizes $n \geq 4$ and $U_0 = 6$. As the forces given by the external potential alternate in sign, we may neglect them compared to the constant drag force, i.e., we roughly estimate the cluster velocity to equal f . This gives $t_\sigma \simeq (1 - \sigma)/f$ and we hence obtain

$$v_d(\sigma) \simeq \alpha \frac{f}{1 - \sigma}. \quad (9)$$

The proportionality factor α should be of the order of one and only weakly dependent on σ . In fact, when choosing $\alpha = 1.35$, we obtain a quite good agreement of the estimate in Eq. (9) with the simulated data, see Fig. 6.

Equation (9) would predict that the defect velocity becomes arbitrary large in the limit $\sigma \rightarrow 1$, i.e. when the particle diameter approaches the wavelength of the cosine potential. However, as explained above, a defect formation requires the formation of a hole as an initial step. A hole can only form for $\sigma < (L - 1)/L$, i.e. the limit $\sigma \rightarrow 1$ cannot be taken in a finite system. The thermodynamic limit $L \rightarrow \infty$ is discussed in the next section.

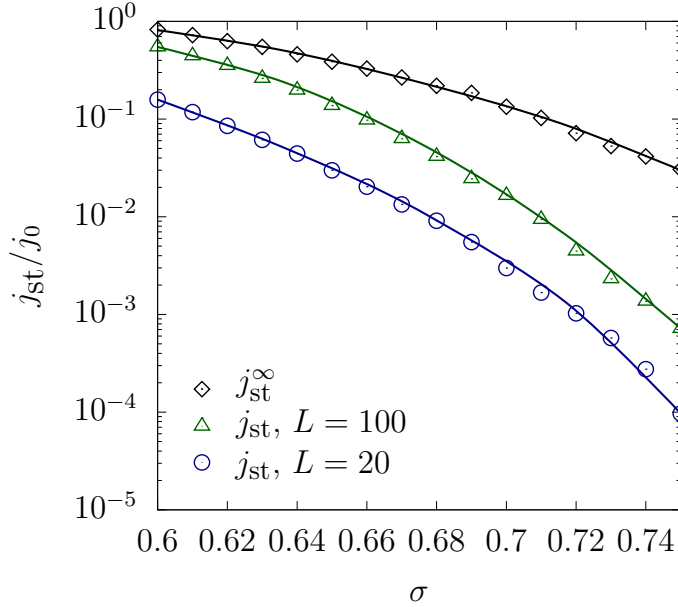


FIG. 7. Steady-state current j_{st} as a function of σ for different system sizes L compared to its value j_{st}^{∞} in the limit $L \rightarrow \infty$. As in Fig. 1, the currents are normalized with respect to the current j_0 of noninteracting particles. The lines are drawn as guide for the eyes.

III. DEFECT-MEDIATED CURRENT

Knowing the defect velocity v_d and generation rate λ_{gen} , we can calculate the defect-mediated current for large systems (thermodynamic limit of infinite system size), where defects are constantly generated and annihilated. Annihilation occurs after some lifetime if a defect encounters a hole. Accordingly, the mean lifetime τ is equal to $\tau = d_h/v_d$, where d_h is the mean distance between holes. This is given by $d_h = 1/\rho_h$, where ρ_h is the number density of holes, which is also the number density of defects, $\rho = \rho_h$. This varies in time as

$$\frac{d\rho}{dt} = \lambda_{\text{gen}} - \frac{\rho}{\tau}. \quad (10)$$

In the steady state, we obtain $\rho_{\text{st}} = \lambda_{\text{gen}}\tau = \lambda_{\text{gen}}/\rho_{\text{st}}v_d$, i.e., $\rho_{\text{st}} = (\lambda_{\text{gen}}/v_d)^{1/2}$. The defect-mediated current in the steady state then is

$$j_{\text{st}}^{\infty} = \rho_{\text{st}} v_d = \sqrt{\lambda_{\text{gen}} v_d}. \quad (11)$$

As shown in Fig. 7, the results predicted by Eq. (11) in the limit of infinite system size do not agree with the simulated data for $L = 20$ and $L = 100$. In particular, the decrease of j_{st}^{∞} with σ is much weaker and it does not resemble an apparent jamming transition.

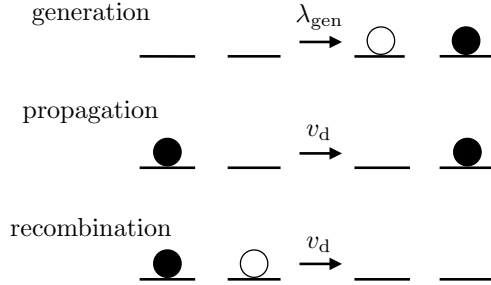


FIG. 8. Possible elementary processes in the coarse-grained lattice model.

The reason for this mismatch is that the current becomes strongly affected by the finite size of system, when L becomes smaller than a distance L_σ proportional to the mean distance $1/\rho_{\text{st}}$ between the defects in the infinite system. In the following, we set $L_\sigma = (v_d/\lambda_{\text{gen}})^{1/2}$. Accordingly, the length L_σ is expected to be very large due to the small rate for the rare events of defect generation. Unfortunately, in the Brownian dynamics simulations of hard spheres at filling factor one and large $\sigma \gtrsim 0.5$, one cannot explore the dynamics at large lengths L in a reasonable computing time due to the large number of collisions between the spheres. These collisions must be treated carefully in the algorithm [31], in particular regarding the choice of a proper integration time step and the treatment of multiple collisions during one time step [42].

Hence, we thought of overcoming this problem by developing a coarse-grained lattice model of the defect dynamics. In this model, illustrated in Fig. 8, particles represent defects and holes represent unoccupied potential wells. A lattice site can be either occupied by a hole or a particle, or it can be empty. Double occupancies of lattice sites by holes and particles are forbidden. The holes cannot move, which reflects that their motion is much slower than that of the defects. The particles can jump to a right nearest-neighbor site with a rate v_d if this site is empty or occupied by a hole. In the latter case, the particle and hole recombine and the site becomes empty. Holes and particles are generated in pairs at nearest-neighbor empty sites with the rate λ_{gen} . This model can be considered as a variant of the two-species totally asymmetric simple exclusion process [43, 44], where the particle-hole generation and recombination are specific features here.

The current in the lattice model is obtained by counting the number of particle jumps per time. In Fig. 9 it is shown how the currents vary with L for different σ . For $L \leq 10^3$ they agree well with the currents of the BASEP, which confirms the proposed mechanism of

defect-mediated currents. The lattice model thus allows to uncover the full dependence on L . For $L \lesssim L_\sigma = 1/\varrho_{\text{st}}$, the current is limited by the low total rate $\lambda_{\text{gen}}L$ of generating defects, hence $j_{\text{st}} \simeq \lambda_{\text{gen}}L$. For $L \gg 1/\varrho_{\text{st}}$, the current approaches j_{st}^∞ given in Eq. (11).

The dependence of $j_{\text{st}} = j_{\text{st}}(\sigma, L)$ on both σ and L can be described by the scaling form $j_{\text{st}}(\sigma, L) = j_{\text{st}}^\infty G(L/L_\sigma)$, or

$$j_{\text{st}}(\sigma, L) = \sqrt{\lambda_{\text{gen}}v_{\text{d}}} G\left(\sqrt{\frac{\lambda_{\text{gen}}}{v_{\text{d}}}}L\right). \quad (12)$$

This scaling is demonstrated in Fig. 9(b), where the simulated data collapse onto the master curve $G(x)$. Because $j_{\text{st}} \simeq \lambda_{\text{gen}}L$ for small L , we must have $G(x)/x \rightarrow 1$ for $x \rightarrow 0$. For $x \rightarrow \infty$, $G(x) \rightarrow 1$. A simple approximate form of the scaling function is

$$G(x) \simeq 1 - e^{-x}. \quad (13)$$

This is shown as the dashed line in Fig. 9(b).

IV. SUMMARY AND CONCLUSIONS

We have shown that an apparent jamming transition occurs in the driven Brownian motion of hard spheres through a periodic potential under a constant drag force f , where the particle number equals the number of potential wells (filling factor one). This jamming transition manifests itself in steady-state currents j_{st} decreasing by several orders of magnitude if the particle diameter σ is increased beyond 0.6 wavelengths of the periodic potential. The current in the apparently jammed states is mediated by defects that are collective thermal excitations.

These defects are appearing as rare events. Determining their properties in many-particle Brownian dynamics simulations is therefore a challenging task. We have obtained reliable results for currents and defect generation rates by direct simulation for system sizes L up to 10^3 wavelengths. For evaluating defect velocities v_{d} , the largest possible L were even much smaller ($L \lesssim 50$). To overcome difficulties with the very rare defect generation, we have applied a particle insertion method for obtaining v_{d} much more efficiently. We have designed a coarse-grained lattice model to fully uncover the current behavior as a function of system size.

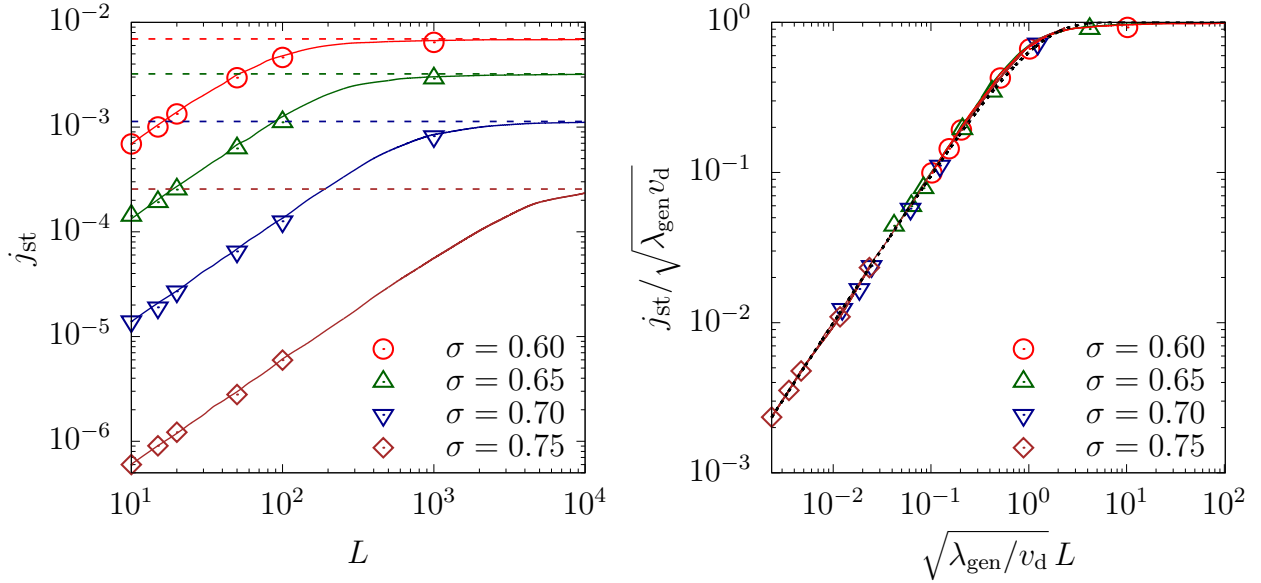


FIG. 9. (a) Dependence of the steady-state current j_{st} on the system size L for various particle diameters σ . The solid lines are from kinetic Monte Carlo simulations of the coarse-grained lattice model, cf. Fig. 8. They agree well with the results from Brownian dynamics simulations (symbols) and for large L approach the theoretically predicted value j_{st}^∞ given in Eq. (11) [indicated by the dashed horizontal lines]. (b) Scaled current vs. scaled system size demonstrating the data collapse onto a common master curve (solid line). The master curve corresponds to the scaling function $G(\cdot)$ in Eq. (12) and the dashed line represents the approximation (13).

To describe the defect generation, we have developed a transition state theory. It predicts defect generation rates λ_{gen} which decay faster than exponentially with σ and are in excellent quantitative agreement with simulations. The number of particles forming the transition state follows from a maximum free energy barrier principle.

The velocity v_d of the defects is hundred times larger than that of a single (noninteracting) particle dragged through the periodic potential, and even several times larger than that of a single dragged particle in the absence of the periodic potential. We have explained this ultrafast defect propagation by considering a coherent-like motion of particles within a defect cluster. The potential amplitude for the cluster dynamics is effectively reduced. By further taking into account geometric relations, we have obtained the approximate expression $v_d \propto f/(1 - \sigma)$.

By combining the results for the defect velocity and generation rate, we have derived a

scaling law for describing the dependence of the currents on σ and the system size L . There are two scaling regimes of small and large L , which are separated by the mean distance L_σ between the defects in the thermodynamic limit, i.e., $L_\sigma = 1/\varrho_{\text{st}}$, where ϱ_{st} is the number density of defects. For small system size $L \lesssim L_\sigma$, the current is governed by the defect generation rate solely, $j_{\text{st}} \simeq \lambda_{\text{gen}}L$. Thus the apparent jamming transition is caused by the strong decrease of λ_{gen} with σ . For large L , $j_{\text{st}} \simeq \sqrt{\lambda_{\text{gen}}v_{\text{d}}}$, meaning that the decrease of j_{st} with σ is much weaker than in the scaling regime of small L .

It is remarkable that the complex rare event dynamics of the defects and their connection to currents could be accounted for by the theoretical concepts introduced above. We believe that the method of identifying many-particle transition states and of calculating their formation rates can be applied to describe the collective motion of current carriers in various crowded systems. The dependence of the defect velocity on the particle size appears to be a typical feature of cluster dynamics. Similarly, the scaling behavior of currents with respect to system size seems to be a generic feature for charge transport in one-dimensional conductors.

Nowadays, many experimental techniques are capable to control and track the motion of microparticles in crowded environments [45–56]. The apparent jamming transition should be well accessible by measurements because it occurs already for particle diameters significantly smaller than the wavelength of the periodic potential. For experiments with colloidal particles confined to channels of optical or magnetic traps, the number of particles is about 10-100. In that range, the apparent jamming transition is particularly pronounced. Moreover, the particle insertion method can be used to study defect propagation in a controlled way and to overcome possible problems with the observation of rare events. Such experiments can critically test the theoretical predictions and possibly uncover new unexplored features of collective excitations in dense many-particle systems.

Acknowledgements

Financial support by the Czech Science Foundation (Project No. 20-24748J) and the Deutsche Forschungsgemeinschaft (Project No. 432123484) is gratefully acknowledged. A part of computational resources was supplied by the project “e-Infrastruktura CZ” (e-INFRA CZ

LM2018140) supported by the Ministry of Education, Youth and Sports of the Czech Republic.

- [1] Q.-H. Wei, C. Bechinger, and P. Leiderer, Single-file diffusion of colloids in one-dimensional channels, *Science* **287**, 625 (2000).
- [2] A. Taloni, O. Flomenbom, R. Castañeda-Priego, and F. Marchesoni, Single file dynamics in soft materials, *Soft Matter* **13**, 1096 (2017).
- [3] A. Schadschneider, D. Chowdhury, and K. Nishinari, *Stochastic Transport in Complex Systems: From Molecules to Vehicles*, 3rd ed. (Elsevier Science, Amsterdam, 2010).
- [4] T. Chou, K. Mallick, and R. K. P. Zia, Non-equilibrium statistical mechanics: from a paradigmatic model to biological transport, *Rep. Prog. Phys.* **74**, 116601 (2011).
- [5] C. T. MacDonald, J. H. Gibbs, and A. C. Pipkin, Kinetics of biopolymerization on nucleic acid templates, *Biopolymers* **6**, 1 (1968).
- [6] A. B. Kolomeisky, Motor proteins and molecular motors: how to operate machines at the nanoscale, *J. Phys.: Condens. Matter* **25**, 463101 (2013).
- [7] C. Appert-Rolland, M. Ebbinghaus, and L. Santen, Intracellular transport driven by cytoskeletal motors: General mechanisms and defects, *Phys. Rep.* **593**, 1 (2015).
- [8] K. Hahn, J. Kärger, and V. Kukla, Single-file diffusion observation, *Phys. Rev. Lett.* **76**, 2762 (1996).
- [9] C.-Y. Cheng and C. R. Bowers, Observation of single-file diffusion in dipeptide nanotubes by continuous-flow hyperpolarized Xenon-129 NMR spectroscopy, *ChemPhysChem* **8**, 2077 (2007).
- [10] M. Dvoyashkin, H. Bhase, N. Mirnazari, S. Vasenkov, and C. R. Bowers, Single-file nanochannel persistence lengths from NMR, *Anal. Chem.* **86**, 2200 (2014).
- [11] W. R. Bauer and W. Nadler, Molecular transport through channels and pores: Effects of in-channel interactions and blocking, *Proc. Natl. Acad. Sci. U.S.A.* **103**, 11446 (2006).
- [12] M. Kahms, P. Lehrich, J. Hüve, N. Sanetra, and R. Peters, Binding site distribution of nuclear transport receptors and transport complexes in single nuclear pore complexes, *Traffic* **10**, 1228 (2009).
- [13] P. C. Bressloff and J. M. Newby, Stochastic models of intracellular transport, *Rev. Mod. Phys.* **85**, 135 (2013).

- [14] B. Derrida, An exactly soluble non-equilibrium system: The asymmetric simple exclusion process, [Phys. Rep. **301**, 65 \(1998\)](#).
- [15] G. M. Schütz, Exactly solvable models for many-body systems far from equilibrium, in *Phase Transitions and Critical Phenomena*, Vol. 19, edited by C. Domb and J. Lebowitz (Academic Press, London, 2001) pp. 1–251.
- [16] R. A. Blythe and M. R. Evans, Nonequilibrium steady states of matrix-product form: a solver’s guide, [J. Phys. A Math. Theor. **40**, R333 \(2007\)](#).
- [17] D. Chowdhury, Stochastic mechano-chemical kinetics of molecular motors: A multidisciplinary enterprise from a physicist’s perspective, [Phys. Rep. **529**, 1 \(2013\)](#).
- [18] S. Pillay, H. M. Byrne, and P. K. Maini, The impact of exclusion processes on angiogenesis models, [J. Math. Biol. **77**, 1721 \(2018\)](#).
- [19] A. Riba, N. D. Nanni, N. Mittal, E. Arhné, A. Schmidt, and M. Zavolan, Protein synthesis rates and ribosome occupancies reveal determinants of translation elongation rates, [Proceedings of the National Academy of Sciences **116**, 15023 \(2019\)](#).
- [20] R. C. Mines, T. Lipniacki, and X. Shen, Slow nucleosome dynamics set the transcriptional speed limit and induce rna polymerase ii traffic jams and bursts, [PLoS Comput. Biol. **18**, 1 \(2022\)](#).
- [21] J. Krug, Boundary-induced phase transitions in driven diffusive systems, [Phys. Rev. Lett. **67**, 1882 \(1991\)](#).
- [22] T. Antal and G. M. Schütz, Asymmetric exclusion process with next-nearest-neighbor interaction: Some comments on traffic flow and a nonequilibrium reentrance transition, [Phys. Rev. E **62**, 83 \(2000\)](#).
- [23] M. Dierl, M. Einax, and P. Maass, One-dimensional transport of interacting particles: Currents, density profiles, phase diagrams, and symmetries, [Phys. Rev. E **87**, 062126 \(2013\)](#).
- [24] D. Lips, A. Ryabov, and P. Maass, Brownian asymmetric simple exclusion process, [Phys. Rev. Lett. **121**, 160601 \(2018\)](#).
- [25] D. Lips, A. Ryabov, and P. Maass, Single-file transport in periodic potentials: The Brownian asymmetric simple exclusion process, [Phys. Rev. E **100**, 052121 \(2019\)](#).
- [26] A. P. Antonov, A. Ryabov, and P. Maass, Driven transport of soft Brownian particles through pore-like structures: Effective size method, [J. Chem. Phys. **155**, 184102 \(2021\)](#).
- [27] E. Cereceda-López, D. Lips, A. Ortiz-Ambriz, A. Ryabov, P. Maass, and P. Tierno, Hydrody-

- dynamic interactions can induce jamming in flow-driven systems, [Phys. Rev. Lett. **127**, 214501 \(2021\)](#).
- [28] C. Scalliet, L. Berthier, and F. Zamponi, Nature of excitations and defects in structural glasses, [Nat. Commun. **10**, 5102 \(2019\)](#).
- [29] A. Huerta, T. Bryk, V. M. Pergamenschchik, and A. Trokhymchuk, Collective dynamics in quasi-one-dimensional hard disk system, [Front. Phys. **9**, 636052 \(2021\)](#).
- [30] Y.-G. Tao, W. K. den Otter, J. K. G. Dhont, and W. J. Briels, Isotropic-nematic spinodals of rigid long thin rodlike colloids by event-driven Brownian dynamics simulations, [J. Chem. Phys. **124**, 134906 \(2006\)](#).
- [31] A. Scala, T. Voigtmann, and C. De Michele, Event-driven Brownian dynamics for hard spheres, [J. Chem. Phys. **126**, 134109 \(2007\)](#).
- [32] A. Scala, Event-driven Langevin simulations of hard spheres, [Phys. Rev. E **86**, 026709 \(2012\)](#).
- [33] H. Behringer and R. Eichhorn, Brownian dynamics simulations with hard-body interactions: Spherical particles, [J. Chem. Phys. **137**, 164108 \(2012\)](#).
- [34] F. Sammüller and M. Schmidt, Adaptive Brownian dynamics, [J. Chem. Phys. **155**, 134107 \(2021\)](#).
- [35] Encounters between two particles in small time steps Δt are treated as elastic collisions. Let Δx_i be the attempted displacement of a particle i in the time interval Δt according to Eq. (1) when ignoring hard-sphere interactions. If that Δx_i in connection with the Δx_j of its neighboring particles does not lead to an encounter of the respective particles, the particle i is displaced accordingly. If particle i would encounter particle j , they are treated as freely propagating hard spheres exchanging their fictive velocities $\Delta x_i/\Delta t$ and $\Delta x_j/\Delta t$, i.e. the displacement of particle i is the result of an elastic collision. If there is a subsequent collision, it is treated analogously.
- [36] A. Ryabov, D. Lips, and P. Maass, Counterintuitive short uphill transitions in single-file diffusion, [J. Phys. Chem. C **123**, 5714 \(2019\)](#).
- [37] A. Antonov, S. Schweers, A. Ryabov, and P. Maass, in preparation.
- [38] D. Voráč, P. Maass, and A. Ryabov, Cycle completion times probe interactions with environment, [J. Phys. Chem. Lett. **11**, 6887 \(2020\)](#).
- [39] R. L. Stratonovich, Oscillator synchronization in the presence of noise, in *Non-linear Transformations of Stochastic Processes*, edited by P. I. Kuznetsov, R. L. Stratonovich, and V. I.

- Tikhonov (Pergamon Press, Oxford, 1965) pp. 269–282, first published in Russian in *Radiotekh. Elektron.* (Moscow) **3**, 497 (1958).
- [40] V. Ambegaokar and B. I. Halperin, Voltage due to thermal noise in the dc Josephson effect, *Phys. Rev. Lett.* **22**, 1364 (1969).
- [41] D. Lips, R. L. Stoop, P. Maass, and P. Tierno, Emergent colloidal currents across ordered and disordered landscapes, *Commun. Phys.* **4**, 224 (2021).
- [42] For example, for the small system size $L = 20$, the CPU time to obtain a single value j_{st} for $\sigma = 0.75$ is about 230 hours on a 16-core Intel Xeon Nehalem 2.66 GHz processor.
- [43] M. R. Evans, D. P. Foster, C. Godrèche, and D. Mukamel, Asymmetric exclusion model with two species: Spontaneous symmetry breaking, *J. Stat. Phys.* **80**, 69 (1995).
- [44] P. Bonnin, I. Stansfield, M. C. Romano, and N. Kern, Two-species totally asymmetric simple exclusion process model: From a simple description to intermittency and traveling traffic jams, *Phys. Rev. E* **105**, 034117 (2022).
- [45] T. Bohlein, J. Mikhael, and C. Bechinger, Observation of kinks and antikinks in colloidal monolayers driven across ordered surfaces, *Nat. Mater.* **11**, 126 (2012).
- [46] A. Vanossi, N. Manini, and E. Tosatti, Static and dynamic friction in sliding colloidal monolayers, *Proc. Natl. Acad. Sci. U.S.A.* **109**, 16429 (2012).
- [47] P. Tierno, Recent advances in anisotropic magnetic colloids: realization, assembly and applications, *Phys. Chem. Chem. Phys.* **16**, 23515 (2014).
- [48] A. V. Arzola, M. Villasante-Barahona, K. Volke-Sepúlveda, P. Jákl, and P. Zemánek, Omnidirectional transport in fully reconfigurable two dimensional optical ratchets, *Phys. Rev. Lett.* **118**, 138002 (2017).
- [49] S. Pagliara, C. Schwall, and U. F. Keyser, Optimizing diffusive transport through a synthetic membrane channel, *Advanced Materials* **25**, 844 (2013).
- [50] S. Pagliara, S. L. Dettmer, and U. F. Keyser, Channel-facilitated diffusion boosted by particle binding at the channel entrance, *Phys. Rev. Lett.* **113**, 048102 (2014).
- [51] M. P. N. Juniper, A. V. Straube, R. Besseling, D. G. A. L. Aarts, and R. P. A. Dullens, Microscopic dynamics of synchronization in driven colloids, *Nat. Commun.* **6**, 7187 (2015).
- [52] E. Locatelli, M. Pierno, F. Baldovin, E. Orlandini, Y. Tan, and S. Pagliara, Single-file escape of colloidal particles from microfluidic channels, *Phys. Rev. Lett.* **117**, 038001 (2016).
- [53] M. J. Skaug, C. Schwemmer, S. Fringes, C. D. Rawlings, and A. W. Knoll, Nanofluidic rocking

- Brownian motors, [Science](#) **359**, 1505 (2018).
- [54] C. Schwemmer, S. Fringes, U. Duerig, Y. K. Ryu, and A. W. Knoll, Experimental observation of current reversal in a rocking Brownian motor, [Phys. Rev. Lett.](#) **121**, 104102 (2018).
- [55] P. Zemánek, G. Volpe, A. Jonáš, and O. Brzobohatý, Perspective on light-induced transport of particles: from optical forces to phoretic motion, [Adv. Opt. Photon.](#) **11**, 577 (2019).
- [56] S. Battat, D. A. Weitz, and G. M. Whitesides, Nonlinear phenomena in microfluidics, [Chem. Rev.](#) [10.1021/acs.chemrev.1c00985](https://doi.org/10.1021/acs.chemrev.1c00985) (2022), PMID: 35194990.